Science Translational Medicine
AAAS

Vitamin D Deficiency Induces Early Signs of Aging in Human Bone, Increasing the Risk of Fracture

Björn Busse *et al.*

Sci Transl Med **5**, 193ra88 (2013);
DOI: 10.1126/scitranslmed.3006286

Editor's Summary

Vitamin D–Deficient Bone Showing Its Age

Vitamin D, which is sometimes called the "sunshine vitamin" because humans can synthesize it in the presence of sunlight, has long been associated with prevention of bone disease. Vitamin D is required for proper absorption of calcium and its uptake into bone, and a lack of vitamin D is known to cause rickets and osteomalacia—diseases in which bone is too soft because of excessive collagenous matrix and its inadequate mineralization. Now, Busse and co-authors provide some evidence that the reverse is also partially true, and vitamin D deficiency can result in areas of overly dense mineralization in the bone.

To study the effects of vitamin D deficiency, Busse and colleagues used samples of bone from 30 apparently healthy people. Half of these subjects were deficient in vitamin D, defined by low concentration of vitamin D in the blood and altered macroscopic characteristics of the bone. Through detailed analysis of bone structure and functional tests measuring the bones' resistance to cracking, the authors characterized the ways in which vitamin D –deficient bone differs from normal. As expected, they found that bones from vitamin D –deficient subjects had a much thicker layer of unmineralized osteoid coating the surface of mineralized bone. However, they also demonstrated that the bone underneath this osteoid layer was more heavily mineralized than normal and had structural characteristics of older and more brittle bone. They explained this phenomenon by noting that osteoclasts, cells that normally remodel the bone, cannot get through the thick osteoid layer. As a result, the areas of bone hidden underneath the osteoid continue to age and mineralize even as the overall bone mineral content progressively decreases.

These interesting and unexpected findings about human bone emphasize the negative consequences of vitamin D deficiency, which is all too common, especially at northern latitudes. Additional work will be needed to translate this knowledge into clinical practice, but the detailed understanding of human bone structure may provide some insight into more effective ways to prevent or treat fractures in patients with vitamin D deficiency.

Science Translational Medicine (print ISSN 1946-6234; online ISSN 1946-6242) is published weekly, except the last week in December, by the American Association for the Advancement of Science, 1200 New York Avenue NW, Washington, DC 20005.

BONE

Vitamin D Deficiency Induces Early Signs of Aging in Human Bone, Increasing the Risk of Fracture

Björn Busse,[1,2]* Hrishikesh A. Bale,[2] Elizabeth A. Zimmermann,[1,2,3] Brian Panganiban,[2] Holly D. Barth,[2,3] Alessandra Carriero,[2] Eik Vettorazzi,[4] Josef Zustin,[5] Michael Hahn,[1] Joel W. Ager III,[2] Klaus Püschel,[6] Michael Amling,[1] Robert O. Ritchie[2,3]

Vitamin D deficiency is a widespread medical condition that plays a major role in human bone health. Fracture susceptibility in the context of low vitamin D has been primarily associated with defective mineralization of collagenous matrix (osteoid). However, bone's fracture resistance is due to toughening mechanisms at various hierarchical levels ranging from the nano- to the microstructure. Thus, we hypothesize that the increase in fracture risk with vitamin D deficiency may be triggered by numerous pathological changes and may not solely derive from the absence of mineralized bone. We found that the characteristic increase in osteoid-covered surfaces in vitamin D–deficient bone hampers remodeling of the remaining mineralized bone tissue. Using spatially resolved synchrotron bone mineral density distribution analyses and spectroscopic techniques, we observed that the bone tissue within the osteoid frame has a higher mineral content with mature collagen and mineral constituents, which are characteristic of aged tissue. In situ fracture mechanics measurements and synchrotron radiation micro–computed tomography of the crack path indicated that vitamin D deficiency increases both the initiation and propagation of cracks by 22 to 31%. Thus, vitamin D deficiency is not simply associated with diminished bone mass. Our analyses reveal the aged nature of the remaining mineralized bone and its greatly decreased fracture resistance. Through a combination of characterization techniques spanning multiple size scales, our study expands the current clinical understanding of the pathophysiology of vitamin D deficiency and helps explain why well-balanced vitamin D levels are essential to maintain bone's structural integrity.

INTRODUCTION

Vitamin D is widespread in nature, and one of its roles in vertebrate animals and humans is to promote the absorption of calcium and phosphate to enable normal mineralization of the skeleton (*1*, *2*). Vitamin D deficiency in childhood makes children prone to rickets, where defective mineralization of growth plate cartilage and bone leads to morphologically altered long bones, resulting in curvature and deformation (*3*, *4*). In adults, vitamin D deficiency causes osteomalacia, a condition of defective mineralization, where newly formed bone matrix (osteoid) fails to mineralize, resulting in bone pain, muscle weakness, and increased risk of bone deformation and fracture (*1*, *4*).

The characteristic feature of a vitamin D deficiency is a low serum 25(OH)D_3 concentration, which is associated with decreases in both serum 1,25-(OH)2D_3 and calcium absorption (*1*, *4*). In turn, low serum calcium results in increased secretion of parathyroid hormone (PTH), which promotes the production of 1,25-(OH)2D_3 (*5*). As a result, serum 1,25-(OH)2D_3 concentrations return to normal but are accompanied by higher serum concentration of PTH, indicative of secondary hyperparathyroidism (*1*, *6*). Increases in serum PTH concentration have been reported to stimulate the rate of bone turnover, causing a reorganization of the bone structure (*1*). Thus, secondary hyperparathyroidism has been accepted as the predominant factor by which vitamin D deficiency results in increased susceptibility to bone fractures (*1*, *7*). Treatment with vitamin D_3 and calcium does result in substantial decreases in nonvertebral fractures. However, this is achieved with only modest increases in bone mineral density (BMD) and variable serum concentrations of PTH, which suggests that other factors play a role in the reduced fracture risk (*1*, *8*).

The hallmark of osteomalacia is an excessive amount of unmineralized collagen matrix (osteoid) (*9*). The cause of this pathological accumulation of osteoid is difficult to determine and may result from a combination of an increased rate of bone formation (*1*, *10*), low serum calcium and phosphorus (*6*, *11*), and/or direct effects of the excess osteoid on osseous cells accompanied by changes in the bone matrix, either in the collagen or in the ground substance (*2*, *12*).

As a consequence of the marked reduction in mineralized bone mass and increased amounts of osteoid, vitamin D–deficient bone represents a complex composite structure that is highly susceptible to fracture (*6*, *13*). However, although correlations between osteomalacic bone and fracture have been reported for vertebral and long bones (*1*, *14*, *15*), a mechanistic understanding of this increased fracture risk remains elusive.

The complexity of morphological/compositional changes in bone and their effects on fracture resistance is due primarily to bone's hierarchical structure, which has characteristic features from near-macroscopic to micrometer to nanometer levels. Specifically, bone evolves to its macroscopic form (>3 mm) from a nanostructure composed of collagen and mineral (<500 nm) and a microstructure of lamellae, osteocyte lacunae (3 to 20 μm), and osteons (100 to 300 μm) (*16*, *17*). Specific aspects that contribute to its fracture resistance originate from widely differing size scales. The intrinsic fracture resistance of bone, which affects both the initiation and growth of cracks, results from "plasticity" at the smallest architectural levels, primarily through sliding of mineralized collagen fibrils. A larger contribution to fracture resistance

[1]Department of Osteology and Biomechanics, University Medical Center Hamburg, D-22529 Hamburg, Germany. [2]Materials Sciences Division, Lawrence Berkeley National Laboratory, Berkeley, CA 94720, USA. [3]Department of Materials Science and Engineering, University of California, Berkeley, CA 94720, USA. [4]Department of Medical Biometry and Epidemiology, University Medical Center Hamburg, D-20246 Hamburg, Germany. [5]Institute of Pathology, University Medical Center Hamburg, D-20246 Hamburg, Germany. [6]Department of Forensic Medicine, University Medical Center Hamburg, D-20246 Hamburg, Germany.
*Corresponding author. E-mail: b.busse@uke.uni-hamburg.de

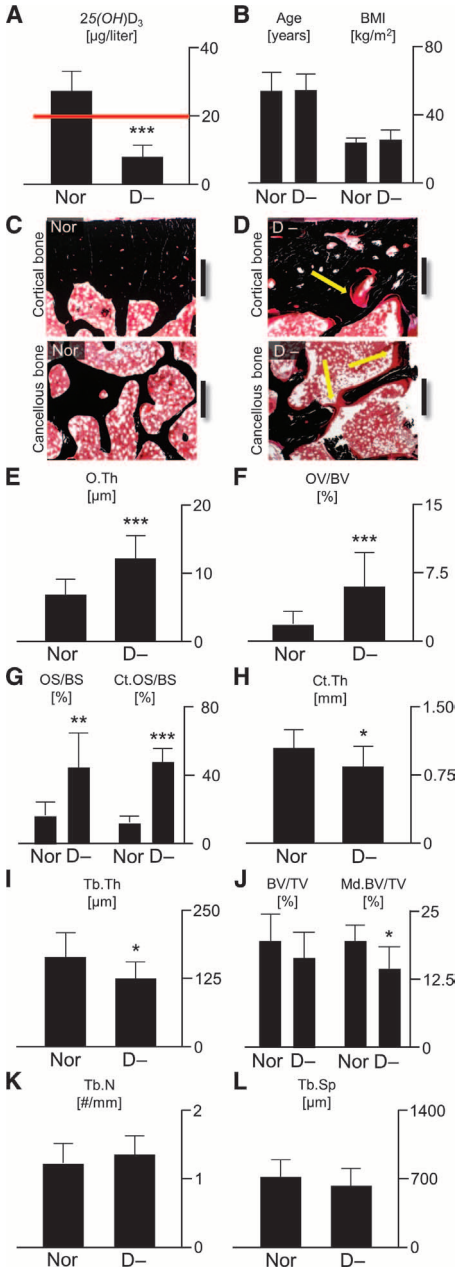

Fig. 1. Characteristics of cases and histomorphometric assessment of static structure indices. (**A**) Serum concentrations of 25(OH)D_3 are shown in vitamin D–deficient subjects (D–) and normal controls (Nor) ($P \leq 0.0001$). The threshold of normal vitamin D concentration (20 μg/liter) is marked with a red line. (**B**) Normal (Nor) and vitamin D–deficient (D–) cohorts were similar in age and BMI. (**C**) Histology of normal bone, showing regular cortical and cancellous bone architecture with no mineralization defects and normal osteoid characteristics. Scale bars, 600 μm. (**D**) Vitamin D–deficient samples showing altered bone structure with prominent osteoid seams (arrows) (black, mineralized bone tissue; red, bone marrow; von Kossa–stained). Scale bars, 600 μm. (**E** to **L**) Histomorphometric values of bone from normal and vitamin D–deficient subjects (mean ± SEM, $n = 15$). The bar graphs show the differences in thickness of osteoid seams ($P = 0.0008$) (E), the ratio of osteoid volume to bone volume ($P = 0.0005$) (F), the ratio of osteoid surface to bone surface in trabecular bone ($P = 0.0008$) and in the cortical bone ($P \leq 0.0001$) that is subsequently subject to the analysis of fracture toughness (G), the cortical thickness ($P = 0.048$) (H), the trabecular thickness ($P = 0.031$) (I), the ratio of bone volume per tissue volume and mineralized bone volume to tissue volume ($P = 0.015$) (J), the trabecular number (K), and the trabecular separation (L) between the study groups.

arises extrinsically from the interactions between the path of cracks and the microstructure of the bone (*16*–*18*); this causes "shielding" of the crack tip from the applied stresses via such mechanisms as crack deflection and bridging, which affect the propagation of cracks. We hypothesize that osseous changes caused by hypovitaminosis D and their corresponding effect on bone fracture are the result of a simultaneous multiscale alteration in structure affecting both the intrinsic and extrinsic fracture mechanisms, rather than solely an imbalance of mineralized and nonmineralized bone quantities.

To address this, we examined iliac crest bone cores from normal and vitamin D–deficient individuals with surface osteoidosis, which marks the intermediary morphologic transition between normal and osteomalacic conditions in vitamin D deficiency and is thus a hallmark event in vitamin D deficiency at the bone tissue level. To evaluate the fracture properties of affected bone, we performed in situ toughness tests on external iliac crest cortices (*16*–*18*) and further examined the resulting crack paths in three dimensions (3D) through high-resolution synchrotron radiation micro–computed tomography (SRμCT), expressly to determine how disease-induced changes in microarchitectural features correlated with extrinsic resistance to crack growth (*16*–*18*). Meanwhile, alterations in the mineral and collagen structure at submicrometer scales were correlated with changes in the intrinsic contribution to bone toughness (*19*–*21*). This combined approach was designed to examine the altered characteristics of vitamin D–deficient bone and discern which specific hierarchical levels of bone structure affect the nature of fracture resistance.

RESULTS

Sample characteristics

The characteristics of the human subjects whose bone cores we analyzed are shown in Fig. 1 (also in tables S1 and S2). An accepted 25(OH)D_3 serum concentration less than 20 μg/liter (*1*, *22*, *23*) and 2D bone structure characteristics classified the test subjects as normal (Nor, $n = 15$) or vitamin D–deficient (D–, $n = 15$) (Fig. 1A). The two groups had a similar mean age and body mass index (BMI) (Fig. 1B). Subjects from the control group did not show any abnormal osteoid characteristics that would suggest mineralization defects (Fig. 1C), whereas those in the vitamin D–deficient group showed altered osteoid indices, with abnormally high ratios of osteoid surface per bone surface (OS/BS > 20%) and/or osteoid thickness (mean O.Th > 12 μm) (Fig. 1, D to G) (*1*). The noticeable surface osteoidosis in vitamin D–deficient subjects corresponded to an increased ratio of cortical osteoid surface per bone surface (Ct.OS/BS > 40%) and confirmed the correct assignment of the study groups (Fig. 1G).

Histomorphometric changes of static structure indices

Vitamin D–deficient bone has a structure distinct from that of normal bone, including prominent osteoid seams (Fig. 1, C and D) with a

substantially higher thickness than normal (Fig. 1E). Furthermore, the ratio of osteoid volume per bone volume (OV/BV) in vitamin D–deficient subjects is more than three times the normal (Fig. 1F), whereas the proportion of cancellous and cortical bone surface covered by osteoid are both higher by more than twofold (Fig. 1G) compared to healthy bone with normal mineralization (*1*, *22*, *23*). Thus, all vitamin D–deficient samples demonstrated an increase in surface osteoid, a hallmark of vitamin D deficiency, which was evident at the bone level even in the absence of full-blown osteomalacia. The histomorphometry also showed that the cortical and trabecular thicknesses were almost 20 and 25% lower, respectively, in the presence of vitamin D deficiency (Fig. 1, H and I). The ratio of total bone volume (including osteoid and mineralized bone) per tissue volume (BV/TV) was not significantly different in the two groups, whereas the proportion of mineralized bone volume per tissue volume (Md.BV/TV) was significantly reduced ($P = 0.015$) (Fig. 1J). The trabecular number (Tb.N) (Fig. 1K) and separation (Tb.Sp) (Fig. 1L) did not show differences between the groups.

SRμCT assessment of bone structure

The SRμCT analysis of the external cortex revealed the Haversian canal network in the cortical compartment (Fig. 2, A and B, and table S3). The cortical porosity (Ct.Po) was almost two times higher in the presence of vitamin D deficiency (Fig. 2C). This difference in porosity was not associated with Haversian canal density (Ha.Ca.Dn) (Fig. 2D) but correlated with a 65% increase in Haversian canal diameter (Ha.Ca.Dm) (Fig. 2E). Consistently, the Haversian canal volume per tissue volume (Ha.Ca.V/TV) was two times larger with vitamin D deficiency (Fig. 2F). Such increases in cortical porosity and widening of Haversian canals reflect the defective mineralization of osteoid with surface osteoidosis.

The osteocyte lacunar morphology also contributed to the cortical porosity (Fig. 2, G and H). Although the osteocyte lacunar density (Ot.Lc.Dn) was similar in both cases (Fig. 2I), the osteocyte lacunar volume (Ot.Lc.V) was 14% higher in vitamin D–deficient bone (Fig. 2J). The number of hypermineralized lacunar occlusions, a sign of impaired remodeling below the bone surface, was also increased in vitamin D–deficient bone, reaching double the number seen in controls (1.87 ± 1.28 #/mm^2 compared to 0.85 ± 0.42 #/mm^2; $P = 0.035$). An increased osteocyte lacunar size (*24*–*26*) has been associated with calcium deficiency in other clinical conditions (*27*) and thus represents a further cellular connection between the observed mineralization defects and the function of the mineralized bones.

Bone mineral density distribution assessed by synchrotron radiation

The bone mineral density distribution (BMDD) and the overall weight percentage (wt %) of calcium (Ca) in the bone were assessed via x-ray attenuation on a 3D bone volume (BV) (Fig. 3A and table S4) within the cortical external cortex. The mean and peak calcium weight percentages (Ca Mean and Ca Peak, respectively) were both 10% higher in vitamin D–deficient bone (Fig. 3, B and C); this increase in the percentage of Ca is consistent with an advanced tissue age (defined as osteon age relative to the surrounding tissue) within the osteoid boundaries. Further analysis of the calcium distribution supports the notion of an advanced tissue age. Specifically, we found that the vitamin D–deficient tissue contained less bone with a low mineral content (Ca Low) (Fig. 3D) and more bone with a high mineral content (Ca High) (Fig. 3E).

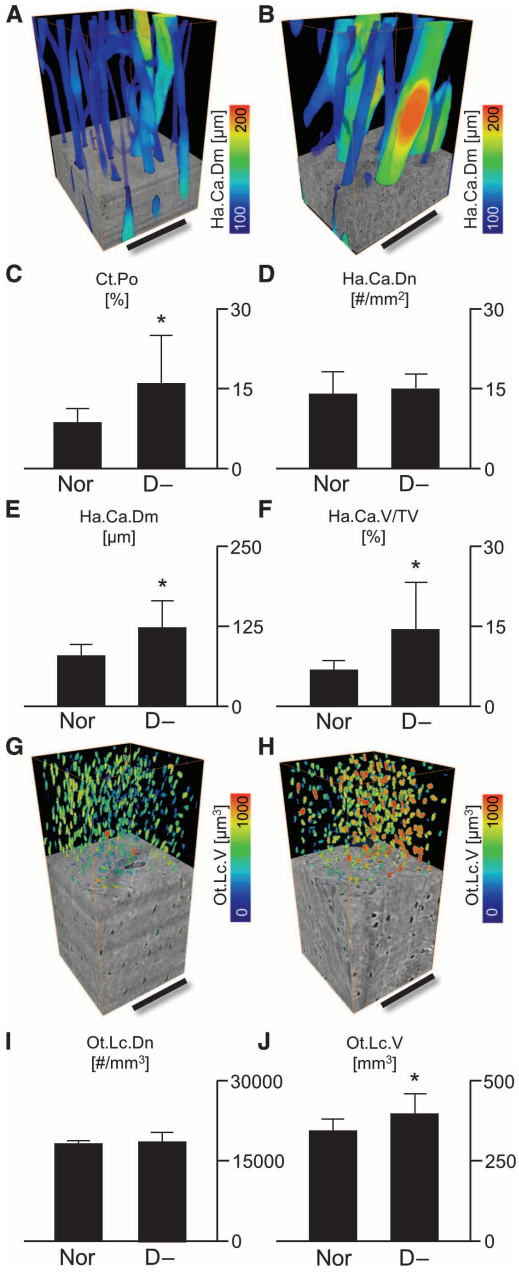

Fig. 2. Tomographic assessment of cortical structure. (**A** and **B**) Micro–computed tomographic images of bone show Haversian canal networks in (A) normal (Nor) bone samples and (B) samples with vitamin D deficiency (D–), where the color scale indicates the haversian canal diameter. Scale bars, 500 μm. (**C** to **F**) Measurements of porosity and Haversian canal structure in normal and vitamin D–deficient samples. Bar graphs show cortical porosity ($P = 0.047$) (C), density of Haversian canals (D), diameter of Haversian canals ($P = 0.008$) (E), and a ratio of Haversian canal volume to tissue volume ($P = 0.037$) (F). (**G** and **H**) Tomographic images demonstrate normal osteocyte lacunae in controls (G) and larger, spherical lacunae in vitamin D–deficient bone (scale bars, 200 μm) (H), where the color scale indicates the osteocyte lacunar volume. (**I**) Osteocyte lacunar density. (**J**) Osteocyte lacunar volume ($P = 0.047$).

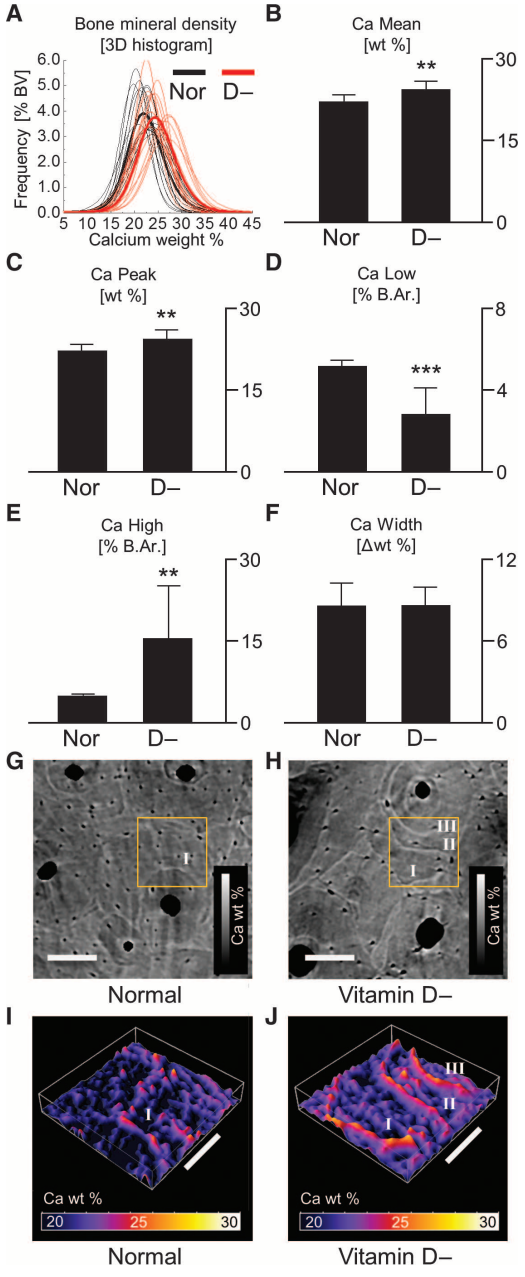

Fig. 3. BMDD by SRμCT. (**A**) Averaged histograms from the 3D volume of cortical bone in the external cortex indicate the extent of mineralization for normal (Nor, black) and vitamin D–deficient (D–, red) bone. (**B** to **F**) Bar graphs depict mean (P = 0.0009) (B) and peak (P = 0.0018) (C) calcium weight percentages, percentages of low mineralized (<5th percentile) bone ($P \leq 0.0001$) (D) and highly mineralized (>95th percentile) bone (P = 0.0034) (E), and calcium width (F), a measure of homogeneity (mean ± SEM, n = 15). (**G** to **J**) Microtomography slices (scale bars, 100 μm) (G and H) and corresponding bone surface plots (scale bars, 50 μm) (I and J) from regions within the yellow boxes depict mineral content and extent of mineralization in both the cement lines (Roman numerals) and bone in normal and vitamin D–deficient samples.

Concurrently, we found that the global heterogeneity of mineralization (Ca Width) was not significantly different between groups (Fig. 3F). Local mineralization profiles (Fig. 3, G and H) and surface plots (Fig. 3, I and J) from individual tomography sections confirmed a higher overall mineralization in both the cement lines and the mineralized portions of vitamin D–deficient bone. A shift toward increased mineralization was also reported in the literature (*28*–*30*).

Spectroscopic characterization of bone collagenous proteins and matrix elements

In areas of mineralized bone (Fig. 4A and table S5), we used vibrational spectroscopy to characterize the collagen and mineral structure/composition and to further confirm the notion of advanced tissue age. Ultraviolet (UV) Raman spectroscopy revealed changes in the amide I band of collagen (Fig. 4B), indicating a change in the cross-linking environment of the collagen, which is also characteristic of aged bone (*31*). Using Fourier transform infrared (FTIR) spectroscopy (Fig. 4C), we determined that the cross-link ratio (*32*), which is associated with collagen maturity, was 20% higher in vitamin D–deficient bone (Fig. 4D). Changes in the carbonate-to-phosphate ratio (Fig. 4E), acid phosphate content (Fig. 4F), and crystallinity (Fig. 4G) were also evident in osteomalacic bone and are all consistent with a maturing mineralization pattern (*33*–*36*).

In situ fracture tests in an environmental scanning electron microscope

Our measurements of fracture toughness with crack resistance curves (R curves) provided evidence as to how multiscale structural changes caused by vitamin D deficiency in external iliac crest bone cortices can explain fracture susceptibility. Measured R curves (Fig. 5A and table S6) revealed a lower fracture resistance in vitamin D–deficient bone, with a 31% decrease in crack initiation toughness, K_o (Fig. 5B), and a 22% decrease in crack growth toughness (Fig. 5C).

At a larger scale, a greater contribution to fracture resistance in bone is derived from extrinsic (crack growth) toughness (Fig. 5C). In normal healthy bone, a major extrinsic toughening mechanism is the deflection of cracks as they encounter the more highly mineralized cement lines (osteonal interfaces) (*16*–*18*). Our 3D x-ray tomographic images (Fig. 5, D and E) indicate an average deflection angle of 68.3 ± 11.2° in controls and an average of 48.5 ± 14.3° in vitamin D–deficient samples (P = 0.003). Such large crack path deflections are a mechanism of delamination (splitting) primarily along the cement lines (Fig. 5D), which toughens normal bone by deviating the crack path from the plane of maximum tensile stress (Fig. 5F). In this way, the stress intensity at the crack tip decreases (typically by a factor of 2 or more) and requires a larger applied force to further propagate the crack (*18*). In vitamin D–deficient bone, conversely, the cement lines no longer represent the most favorable crack path because of osteoidosis-induced morphological changes in osteocyte lacunae and mineral distribution (*27*, *37*); essentially, the large difference in mineral content between the cement line and bone matrix, which drives the crack deflection, is reduced. Consequently, the deflection angle decreases by 30%, and the cracks tend to propagate transversely across the bone and break rather than split it (Fig. 5E), although the crack path remains tortuous (Fig. 5G). Crack deflection along cement lines represents the most effective toughening mechanism in normal bone. The marked differences in crack path seen in vitamin D–deficient bone severely reduce the potency of extrinsic toughening and diminish the role of crack tip shielding, resulting in a considerable reduction in crack growth toughness.

In addition to crack deflection, a second major toughening mechanism in healthy bone involves the formation of uncracked regions

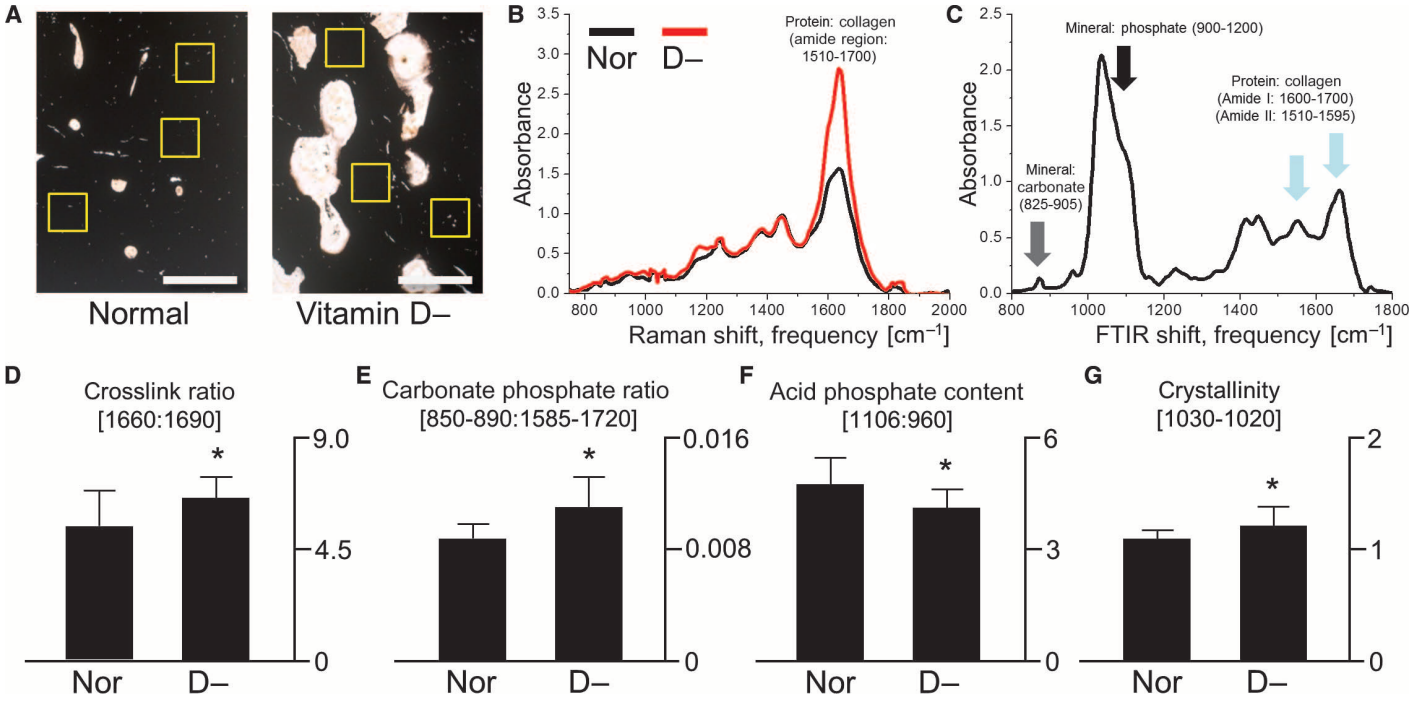

Fig. 4. Spectroscopic characterization of bone collagenous proteins and matrix elements. (**A**) Vibrational spectroscopy was used to analyze regions of interest (yellow boxes) in mineralized bone from each sample. Scale bars, 200 μm. (**B**) Raman spectroscopy indicated changes in the collagenous environment in vitamin D deficiency, seen as differences in the amide I peak. (**C**) FTIR spectra enabled characterization of the matrix properties (mean ± SEM, $n = 15$, representative spectrum shown). (**D** to **G**) The bar graphs present (D) the 1660:1690 peak area ratio, corresponding to collagen maturation ($P = 0.039$); (E) carbonate/phosphate ratio, representing carbonate substitution for phosphate in the mineral lattice ($P = 0.022$); (F) acid phosphate content, marker of overall bone maturity ($P = 0.044$); and (G) crystallinity, representing increased crystal size and perfection ($P = 0.045$).

along the crack path; such "uncracked ligament bridges" have a beneficial effect on bone toughness because the bridges represent intact load-bearing material that would otherwise be used to further crack growth (Fig. 5, F and G, white arrows). Normal bone contained nearly twice as many uncracked ligament bridges as vitamin D–deficient bone (20.1 ± 2.8 compared to 9.75 ± 2.0 bridges, $P \leq 0.0001$), consistent with the pattern seen in aged bone (*16*). Structural changes at multiple size scales advance the tissue age in vitamin D deficiency and impair the extrinsic fracture resistance by limiting the toughening mechanisms of crack deflection and crack bridging, which are prevalent in normal bone. This change in extrinsic resistance is a major factor in the diminished fracture resistance of vitamin D–deficient bone.

DISCUSSION

Although vitamin D deficiency is known to change the bone structure and increase the fracture risk in human cortical bone (*38*), this effect has primarily been attributed to excessive osteoid formation, which causes a decrease in mineralized bone mass. Here, we combined mechanical measurements with histomorphometric evaluation of bone remodeling and characterization of the mineral and collagen components in normal and vitamin D–deficient bone to discern the underlying fracture characteristics associated with osteoidosis. Through this combination of techniques that analyze bone quality at multiple scales, this study has revealed critical aspects of the pathophysiology of vitamin D–deficient conditions.

Because bone is constantly reorganized to adapt to its mechanical and biological environment, we used a histomorphometric assessment to investigate the bone's remodeling status in vitamin D deficiency. Vitamin D deficiency is known to increase the rate of bone turnover to maintain normal calcium levels within the body, producing osteoid that is never mineralized because of the overall calcium imbalance. The deterioration in mechanical properties caused by vitamin D deficiency is associated with a larger amount of osteoid collecting on the osseous surfaces and impairing resorption below the bone surface, as confirmed by the accumulation of nonremodeled hypermineralized osteocyte lacunae (*39*). The mineralized bone framed by osteoid seams cannot be resorbed by osteoclasts through the usual channels (*40*) and is therefore forced to age at the tissue level. In this context, we report an increased degree of mineralization owing to prolonged secondary mineralization in vitamin D–deficient bone. In addition, BMDD and FTIR analyses provide evidence of mature mineral crystals and collagen molecules present within the bone. This conclusion may seem to contradict the reported decreases in mineral content associated with higher osteoid volume and/or undermineralization in vitamin D–deficient bone. However, in most instances, previous conclusions have been based on osteodensitometric (*1*), ash weight (*41*), or other spatially limited measurements, which have the disadvantage of not being able to differentiate between the effect of bone mass versus bone mineralization (*42*). Our current measurements provide 3D spatially resolved BMDDs to differentiate changes in mineralization, independent of overall bone mass, and show that the mineral content may indeed increase with vitamin D deficiency, suggestive of an advanced tissue age. This

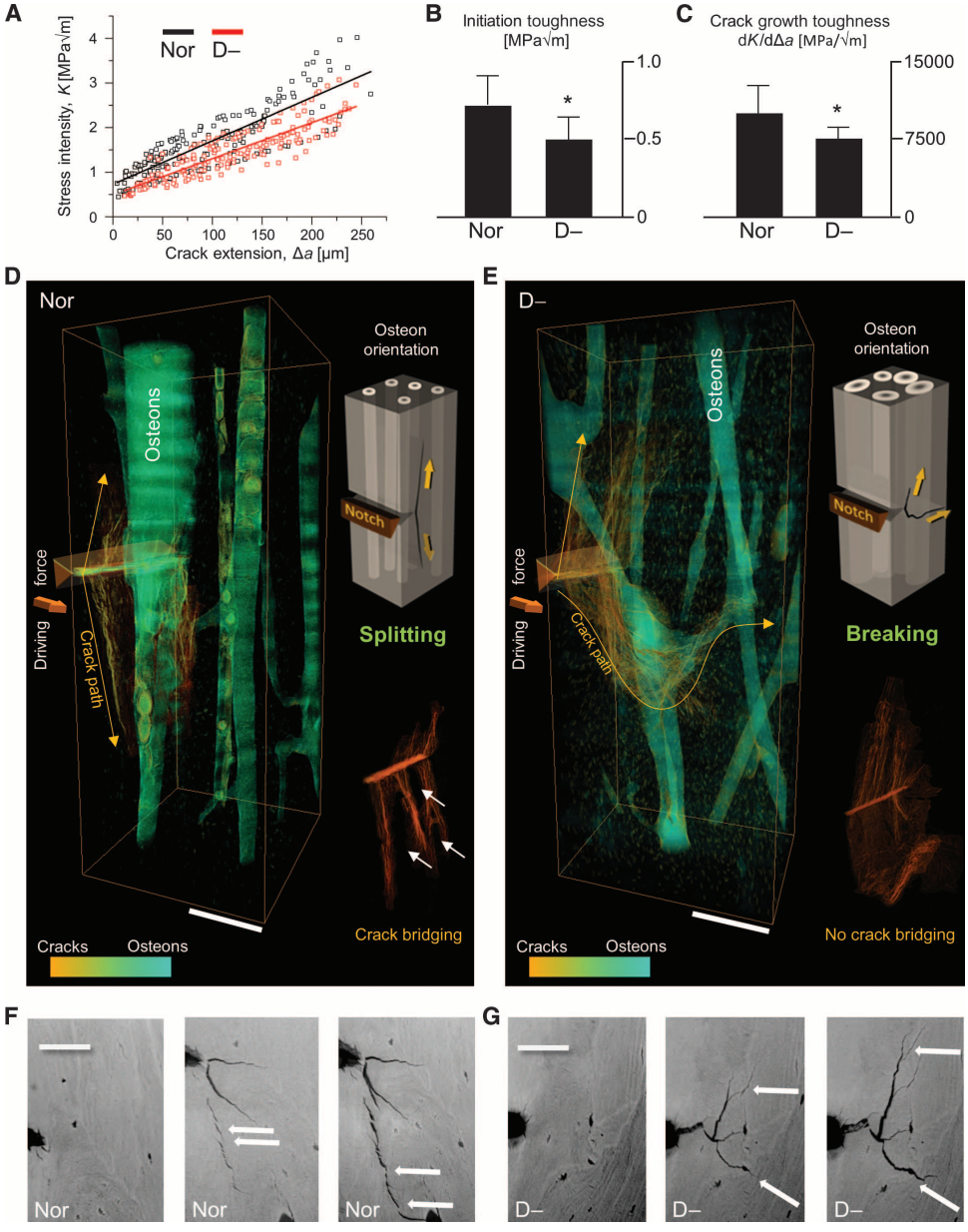

Fig. 5. Mechanical properties and nature of fracture in external iliac crest cortices. (**A**) In vitro fracture toughness *R* curves for human cortical bone in normal (Nor) and vitamin D–deficient (D–) samples. (**B** and **C**) From the *R* curves, the bar graphs depict (B) initiation toughness ($P = 0.046$) and (C) crack growth toughness ($P = 0.049$) (mean ± SEM, $n = 10$). (**D**) 3D reconstruction of the crack path via SRμCT shows pronounced crack deflection by splitting along the interfaces of the osteons in normal bone accompanied by the usual formation of crack bridges. Scale bar, 200 μm. (**E**) In vitamin D–deficient samples, the crack takes a tortuous breaking path across the osteons between the highly mineralized bone and cement lines. Scale bar, 200 μm. This trajectory minimizes the formation of "uncracked ligament" bridges. (**F** and **G**) Images of the crack path during toughness measurements in the environmental scanning electron microscope are shown for normal (F) and vitamin D–deficient (G) bone. The white arrows indicate the formation (F) and absence (G) of uncracked ligament bridges, a major toughening mechanism.

conclusion is in agreement with previous kinetic, histologic, and histomorphometric studies, where a higher mineral content and/or sclerotic changes have been reported in osteomalacic conditions in both humans and animals (*28*, *30*, *43*).

We suggest that local tissue aging is a key cause of increased fracture risk in vitamin D–deficient osteomalacia, contrary to previous beliefs that the increased osteoid volume was the main contributor associated with weakening of the bones. In general, osteoclast precursors (bone-resorbing cells) have been reported to attach only to mineralized tissue (*40*), and thus, the increased osteoid at the internal bone surfaces (such as cancellous surfaces and Haversian canals) may result in less contact surface for osteoclasts to maintain the remodeling process. Tunneling resorption has been previously observed as an alternative pathway for osteoclasts to remove calcified matrix from the inner surface of osteoid, but this resorption pattern has only been reported in severe cases of osteomalacia (OS/BS > 60 to 80%) (*44*) and was not observed in our study group (mean OS/BS ≈ 40%). Consequently, the bone within the osteoid frames has the characteristics of higher tissue age because it is largely excluded from the remodeling process. Frost has previously proposed that in osteomalacia, the total amount of bone-forming and mineralizing sites may actually be greater than in normal bone, whereas the rate of mineralization of individual osteons is reduced (*45*). Because those osteons mineralize slowly, the increase in the number of simultaneously mineralizing osteons may be so great as to actually increase the total rate of mineralization (*30*, *45*). In this paradoxical situation, osteomalacia (defective mineralization) is actually associated with an increase in the rate of total mineral deposited in the bones. This agrees with the findings of Dempster and coworkers (*28*), who showed that individual mineralization clusters in the osteoid and adjacent sites at the edge of mineralized bone matrix were formed much earlier than in normal conditions in the setting of an osteomalacia model. Moreover, the bone in rachitic/osteomalacic conditions was found to be older and more highly mineralized than in control patients with normal vitamin D levels (*28*). Consequently, bone-forming sites with lower mineral content are absent in vitamin D deficiency because of prolonged osteon life spans and decreased osteoblast activity (*45*). Meanwhile, those osteons/bone packets that are already mineralized continue to increase their mineral content during secondary mineralization, leaving the tissue within the osteoid frame with an effective higher tissue age. This change can be

detected at the matrix level by FTIR analyses, where both the higher amide I vibration and the cross-link ratio of vitamin D–deficient bone indicate an aging collagen (*20*, *31*, *36*, *46*). Likewise, in the mineral, we found an increase in carbonate content, which is an essential prerequisite to reach a degree of mineralization (that is, increased Ca/P ratio or increased Ca weight percent) greater than the normal apatitic value (*28*). Thus, we find evidence that impaired remodeling associated with vitamin D deficiency implies an advanced tissue age of the mineral and collagen components of bone, which is also evident in spatially resolved FTIR mappings (fig. S1).

Changes in toughness in normal compared to vitamin D–deficient bone originate from morphological changes in structure that influence how the material absorbs energy during deformation and subcritical fracture. A decrease in initiation toughness results from a decrease in the intrinsic resistance to fracture associated with structural changes at the smallest dimensions. In particular, aging at the tissue level in vitamin D–deficient bone restricts deformation at the submicrometer scale, where bone primarily deforms because of fibrillar sliding (specifically, increased cross-linking in the collagen limits its deformability) (*17*). This diminished plasticity in vitamin D–deficient bone leads directly to a lower intrinsic toughness, identical to that seen with aged human bone (*16*, *17*). Porosity also increases with vitamin D deficiency through an increase in Haversian canal size and osteocyte lacunar volume. Although the influence of porosity on the crack path is difficult to determine, it may contribute to the deterioration in fracture toughness in addition to the changes in mineralization. However, we believe that tissue aging has a predominant effect on the bone's ability to absorb energy by restricting its plasticity, as evidenced by the 31% decrease in crack initiation toughness in vitamin D–deficient bone with surface osteoidosis. Additionally, at higher scales, the mechanisms that toughen bone by altering the path of a growing crack are severely curtailed in vitamin D–deficient bone. This alteration causes the bone to break rather than split, and consequently degrades the crack growth toughness of vitamin D–deficient bone by ~22%.

The study has a few limitations. First, because this study is based on a cross-sectional design, we cannot follow the characteristics within the same individual during periods of vitamin D deficiency or observe the onset of vitamin D deficiency. Human bone tissue has an underlying wide intraindividual heterogeneity; therefore, the limited number of samples may underrepresent the variety of specific bone tissue characteristics. The external cortices taken from iliac crest bone cores were small; larger samples would have allowed us to monitor crack growth at longer crack extensions, where extrinsic crack wake effects have a larger effect on the toughness. Additionally, in many clinical cases, the effects of osteomalacia and osteoporosis can become inseparable and reinforce each other; however, our control and study group showed unchanged bone volume per tissue volume and an increased accumulation of osteoid, which are both hallmarks of vitamin D deficiency.

In summary, we discovered a vicious circle: At first, a state of secondary hyperparathyroidism caused by vitamin D deficiency promotes high bone turnover on mineralized surfaces; mineralized surfaces are thus remodeled at high speed, but the newly deposited osteoid remains unmineralized. As the ratio of osteoid surface per bone surface increases, the corresponding bone surface that can participate in remodeling progressively decreases. Consequently, as the osteoid increases, the calcium balance becomes more and more endangered, but the tissue within the osteoid frame cannot be resorbed and thus is subject to aging. Vitamin D deficiency thus creates a paradox. The mineralized tissue ages despite an endocrine state that promotes high turnover and resorption of old bone. Because of the coating of the bone with resorption-resistant osteoid, vitamin D deficiency causes aging of the tissue and compromises its structural integrity and resistance to fracture. Through the characterization of human bone samples, our study reveals critical aspects of the pathophysiology of vitamin D deficiency. In particular, the spatially resolved analyses of bone quality expand the understanding of tissue-level characteristics of vitamin D deficiency and their contribution to fracture risk. Well-balanced vitamin D levels are essential to maintain bone's structural integrity.

MATERIALS AND METHODS

Study design and cohort

A cohort of control and vitamin D–deficient samples was chosen from a collection of Bordier bone cores taken at the Department of Forensic Medicine, University Medical Center Hamburg-Eppendorf, Germany (*9*, *47*), for a multiscale characterization of bone quality through a suite of experiments. This cross-sectional study was approved by the Medical Association Ethics Committee of the State of Hamburg (OB-024/05) and Lawrence Berkeley National Laboratory (BUA-120).

Subjects were, independent of sex (15 females and 15 males), arranged into two groups: Those with a $25(OH)D_3$ serum concentration less than 20 μg/liter (*1*, *22*, *23*) were classified as vitamin D–deficient ($n = 15$), whereas those with greater than 20 μg/liter were classified as normal ($n = 15$). Because all specimens were taken during full autopsy, all individuals suffering from cancer, renal disease, primary hyperparathyroidism, and Paget's disease or showing any other circumstances, such as immobilization or hospitalization, that could lead to secondary bone disease were excluded from the study (*9*, *42*). The different circumstances leading to death were motor vehicle or train accidents, assaults, suicides, and other unnatural or unexpected causes. In all cases, bone specimens were obtained within 48 hours of death to minimize the postmortem autolysis.

From this group of control and vitamin D–deficient samples, a cohort was chosen for mechanical property measurements. Sample size was only selected to assess the primary endpoint, which was here the fracture mechanics experiment. Previous data from fracture experiments were used to estimate the number of samples needed to investigate toughness changes (*31*); a sample size of $n = 10$ was found to be sufficient for the desired fracture mechanics tests in this study. Blinding was not feasible for this study because of evident macroscopic differences in the bone samples from the two study groups.

For the toughness measurements, all bone cores had to fulfill specific requirements to create standardized samples with no damage or preparation artifacts, to ensure a valid comparison. Thus, all samples (external iliac crest cortices) used for this testing were required to have dimensions of about 12 mm in length and larger than 1.3 mm in width to guarantee a general accordance with the American Society for Testing and Materials Standard ASTM E1820. In addition, only samples without preparation artifacts or damage sustained during biopsy obtainment, grinding, cutting procedures, etc., were used to avoid any nonbiological sources of error in biomechanical testing. After these requirements were fulfilled, we identified 30 applicable samples (15 females and 15 males) for this study.

Laboratory analysis of 25-hydroxyvitamin D

Blood samples were taken on the day of the autopsy. The blood was centrifuged the same day, and the collected serum was stored at −80°C

for further analysis. Serum concentrations of 25(OH)D_3 were measured for all cases at the Department of Clinical Chemistry, University Medical Center Hamburg-Eppendorf, Germany, with a radioimmunoassay (DiaSorin) with an interassay coefficient of variation between 8.2 and 11%. The limit of detection for this method is 1.5 mg/liter. Unlike PTH or calcium, 25(OH)D_3 was found to be stable for at least 10 days postmortem (*9*).

Transiliac crest bone cores

The transiliac crest bone cores were taken at the standard site for bone biopsies, 20 mm below the iliac crest and 20 mm behind the anterosuperior iliac spine, as initially described by Bordier *et al.* (*48*). The samples consisted of outer and inner cortices and the intervening cancellous bone. Specimens were fixed in 3.7% formaldehyde for 3 days, dehydrated, and embedded undecalcified in methyl methacrylate (*9*, *42*). The sections for histology and FTIR were removed with a rotation microtome (microTec, Techno-Med GmbH) from the whole bone core; then, one external cortex was removed with a saw for mechanical testing and tomography.

Histology

After microtome preparations, 4-mm sections were stained with toluidine blue, trichrome Goldner, and a combination of the von Kossa and van Gieson methods, thereby staining mineralized bone matrix black and nonmineralized osteoid red for 2D histomorphometry (*9*, *42*).

2D histomorphometry

Histologic and histomorphometric analyses were performed on trabecular bone with a Zeiss microscope (Carl Zeiss Vision GmbH) and the semiautomatic image-analyzing computer programs OsteoMeasure (OsteoMetrics Inc.) and Bioquant (Bioquant Image Analysis Inc.) according to the American Society for Bone and Mineral Research guidelines (*49*).

3D histomorphometry by SRμCT

External cortical bone specimens from the Bordier bone cores were assessed by microtomography. Regions of interest contained exclusively cortical bone without the subcortical compartment (*50*). SRμCT was performed at the Advanced Light Source (ALS) (beamline 8.3.2) at the Lawrence Berkeley National Laboratory on previously tested *R* curve specimens to ensure that radiation damage did not affect the mechanical properties (*19*). The *R* curve tests were stopped before complete failure of the samples such that the initiated crack path could be preserved.

Stiff adhesive putty (3M 860 Adhesive Putty, 3M Corp.) was used to position the samples upright onto a sample holder. Initial coarse centering of the sample was achieved on an offline microscope-assisted centering stage before placement on the microtomography sample stage. Microtomography scans were conducted at 17 keV with monochromatic x-rays from a four-crystal monochromator at a minimum sample-to-detector distance of 50 mm and a 600-ms exposure at a 1.8 μm/pixel spatial resolution covering 3.8 mm of the sample's length centered around the crack path. The proximal sample-to-detector distance reduced phase-contrast artifacts. Tomography slices were reconstructed with Octopus (Octopus v8, IIC UGent) from 1440 exposures acquired over 180° sample rotation in 0.125° angular increments and visualized in Avizo 6.1 (Visualization Sciences Group Inc.). Reconstructed 16-bit grayscale image data sets consisted of 2150 slices each with 1000 × 1000 pixels. Quantitative analyses of the morphological features in the bone specimens were computed with the quantification software package BoneJ (*51*) within the image analysis software ImageJ (*52*). Before quantification in BoneJ, the data sets were processed by masking the grayscale values of the sample background and Haversian canal cavities and binarizing the data based on grayscale thresholds pertaining to osteocyte lacunae and Haversian canals, respectively.

All external cortices were imaged with synchrotron microtomography after mechanical testing. A roughly 0.5-mm^3 area around the crack tip was used to obtain BMDD information on a 3D volume from each bone sample. Grayscale values of the reconstructed data set directly represented the x-ray mass attenuation coefficients, which were converted to a weight percentage of calcium content at a given spatial location within the 3D volume based on the following formula:

$$\mu_m = \sum_i W_i \mu_{m,i}$$

where μ_m is the mass attenuation (or absorption) coefficient and W_i is the weight fraction of the *i*th component in a multicomponent material containing *i* constituent components. Quantitative measurements of the BMDD of each specimen were determined from histograms constructed with grayscale values of all the pixels enclosed in the mineralized bone volume, excluding the volumes occupied by osteocyte lacunae and Haversian canals. Different parameters of BMDD were determined from the 3D histogram data (*21*).

Raman spectroscopy

Coplanar polished external cortices were assessed by deep UV Raman spectroscopy. The method has been previously published in detail elsewhere (*20*). A continuous wave, intracavity-doubled argon ion laser operating at 244 nm was used as the excitation source for the UV Raman spectroscopy. To avoid damaging the cortical bone matrix, the samples were kept spinning continuously, whereas the excitation source had a ~500-μm spot on the sample surface. Reported data were obtained at 30 cm^{-1} instrument resolution. Spectral calibration was performed with the known Raman line positions of cyclohexane. Five spectra were acquired and averaged for each bone sample. A small linear background was defined by the signal at 500 and 2000 cm^{-1} and subtracted. Spectra were normalized to the height of the CH_2 wag peak at 1460 cm^{-1} and smoothed with a nine-point running average.

FTIR spectroscopy

FTIR spectroscopy was performed at the ALS (beamline 1.4.3) to assess the degree of enzymatic cross-linking in the collagen and the mineral characteristics (*19*). Because the bulk material is not suitable for the FTIR technique, parallel 5-μm-thick sections from the Bordier bone cores were prepared for FTIR analysis in transmission mode. These were embedded in polymethyl methacrylate (PMMA) and then processed to undecalcified histological slices. The sections were left unstained and fixed with dispersion binder on a custom-made aluminum sheet for microanalysis. All FTIR spectroscopy data were obtained from three regions of interest within mineralized bone with a conventional Globar IR source at the ALS. Image spectroscopy consisted of a source, a sample handling unit, and a focal plane array detector on an IR microscope. The recorded spectra were taken in transmission mode with 128 scans and had a spectral resolution of 4 cm^{-1} and a spot size of <150 μm. OMNIC software (Thermo Fischer Scientific)

was used for data processing. After subtraction of PMMA, spectra were curve-fit with a commercially available software package (PeakFit, Systat Software). The initial position and type (Gaussian) of underlying bands were determined through second derivative and difference spectroscopy. The following parameters (*34*, *36*, *51*) were calculated: The cross-link ratio is the relative percent area ratio of two subbands at 1660 and 1690 cm^{-1}; the carbonate-to-phosphate ratio (carbonate substitution for phosphate in the mineral lattice) is defined as the ratio of the integrated area of the carbonate peak (850 to 890 cm^{-1}) to the phosphate area (900 to 1200 cm^{-1}); the acid phosphate content (marker of overall bone maturity) is the percent area ratio of the 1106 and 960 cm^{-1} subbands; and the crystallinity (increased crystal size and perfection) is the area ratio of phosphate subbands at 1030 and 1020 cm^{-1}.

Additionally, the synchrotron source at the ALS (beamline 5.4.1) was used to collect a map of the FTIR spectra in regions of interest. A 15 × 15–μm aperture was used to collect spectra at 5-μm steps. The recorded spectra were taken in transmission mode with 128 scans and had a spectral resolution of 4 cm^{-1}. In the FTIR maps, an additional parameter, termed "mineral maturity," was assessed. The mineral maturity is a parameter recently described by Farlay *et al.* as the ratio of well-crystallized apatite to poorly crystallized apatite and defined as the area ratio of the 1030 to 1110 cm^{-1} subbands. The mineral maturity is a measure of tissue age (*35*).

In situ fracture toughness testing

The external cortical bone was removed from the iliac crest human bone cores with a low speed saw. The external cortices were then polished to their final dimensions with successive grit to a final polish with 5-μm diamond solution. A sharp micro-notch (representing the worst-case flaw) was introduced into the rectangular sample with a low-speed saw, such that the orientation of the osteons was perpendicular to the notch. The root of the saw-cut notch was polished with a razor blade that was irrigated with 0.5-μm diamond solution to a final reproducible crack tip radius of roughly 10 μm. The samples were hydrated in 25°C Hanks' balanced salt solution for at least 12 hours before testing.

The hydrated biopsy samples were subjected to three-point bending in a Gatan Microtest mechanical testing stage at a displacement rate of 0.1 mm/min. The testing was performed in a Hitachi S-4300SE/N environmental scanning electron microscope (Hitachi America), such that crack propagation could be observed while simultaneously measuring the toughness. Images were taken during testing in backscattered electron mode in a vacuum of 35 Pa and a voltage of 25 kV.

During testing, images were taken as the crack extended stably, and the corresponding load value was recorded. In this way, the toughness of the bone was measured as a function of crack extension (the crack growth resistance or *R* curve), in general accordance with the American Society for Testing and Materials Standard ASTM E1820 (*52*). The stress intensity was calculated as follows:

$$K_i = \frac{P_i S}{BW^{3/2}} f(a_i/W)$$

where P_i and a_i are the instantaneous applied load and crack length; S is the length of the loading support span in three-point bending; B and W are the sample thickness and width, respectively; and $f(a/W)$ is a dimensionless function of crack size and sample geometry, which is tabulated in the standard (*52*).

Because crack deflection is a major toughening mechanism in this orientation, the stress intensity values were corrected by the average deflection angle in each specimen measured via 3D SRμCT. Thus, the globally applied mode I stress intensity, K_I, was converted to the local mode I, k_1, and mode II, k_2, stress intensities at the crack tip by the following relationship for in-plane tilted cracks:

$$k_1 = a_{11}(\theta)K_I + a_{12}(\theta)K_{II}$$
$$k_2 = a_{21}(\theta)K_I + a_{22}(\theta)K_{II}$$

where $a_{ij}(\theta)$ are mathematical functions dependent on the angle of crack deflection, θ (*53*). The local stress intensities were then converted to an effective stress intensity by the following relationship:

$$K_{eff} = \sqrt{k_1^2 + k_2^2}$$

The resulting *R* curve provides an assessment of the fracture toughness in the presence of subcritical crack growth because it quantifies the crack driving force, that is, the stress intensity K as a function of crack extension (Δa). The value of K at $\Delta a \rightarrow 0$ provides a measure of the crack initiation toughness, K_o, whereas the slope of the *R* curve can be used to characterize the crack growth toughness.

The samples' size is critical to the validity of the fracture mechanics test. To determine whether plane strain conditions exist, the sample thickness, B, should meet the condition $B > 2.5\ (K/\sigma_Y)^2$, where K is the toughness of the material and σ_Y is the yield stress. On the basis of the average initiation toughness value measured here of roughly 0.72 MPa√m and the average yield stress of bone of around 100 MPa, the thickness should be greater than 0.13 mm. Thus, the sample thicknesses ensured plane strain conditions.

For the K calculation to be valid, the in-plane sample dimensions (that is, crack length and sample width) must be greater than the plastic zone size, r_y. For plane strain conditions, the plastic zone size can be estimated as $r_y \approx 1/6\ (K/\sigma_y)^2$. For our case, the plastic zone size is $r_y = 0.003$ mm, which is a few orders of magnitude smaller than the average width and the average crack length. This represents a condition of "small-scale yielding," which implies that the *K*-field approach to characterize the fracture toughness with these specimen sizes is completely valid.

Statistical analysis

Results are presented as means ± SEM. Statistical analysis was performed with OriginPro 8 (OriginLab Inc.). To test for differences between the study groups, we used the unpaired two-sided *t* test on the normally distributed data. Normal distribution of the data was tested with Kolmogorov-Smirnov test. *P* values ≤0.05 were considered statistically significant.

SUPPLEMENTARY MATERIALS

www.sciencetranslationalmedicine.org/cgi/content/full/5/193/193ra88/DC1
Fig. S1. FTIR spectroscopy mapping.
Table S1. Characterization of study subjects.
Table S2. Histomorphometric assessment of static structure indices.
Table S3. Tomographic assessment of cortical structure.
Table S4. BMDD by SRμCT.
Table S5. Spectroscopic characterization of bone collagenous proteins and matrix elements.
Table S6. Mechanical properties and nature of fracture in external iliac crest cortices.

REFERENCES AND NOTES

1. P. Lips, Vitamin D deficiency and secondary hyperparathyroidism in the elderly: Consequences for bone loss and fractures and therapeutic implications. *Endocr. Rev.* **22**, 477–501 (2001).
2. H. F. DeLuca, Overview of general physiologic features and functions of vitamin D. *Am. J. Clin. Nutr.* **80**, 1689S–1696S (2004).
3. F. Rauch, E. Schoenau, Skeletal development in premature infants: A review of bone physiology beyond nutritional aspects. *Arch. Dis. Child. Fetal Neonatal Ed.* **86**, F82–F85 (2002).
4. M. P. Whyte, R. V. Thakker, Rickets and osteomalacia. *Medicine* **33**, 70–74 (2005).
5. S. Boonen, H. A. Bischoff-Ferrari, C. Cooper, P. Lips, O. Ljunggren, P. J. Meunier, J. Y. Reginster, Addressing the musculoskeletal components of fracture risk with calcium and vitamin D: A review of the evidence. *Calcif. Tissue Int.* **78**, 257–270 (2006).
6. M. F. Holick, Vitamin D deficiency. *N. Engl. J. Med.* **357**, 266–281 (2007).
7. A. M. Parfitt, D. S. Rao, J. Stanciu, A. R. Villanueva, M. Kleerekoper, B. Frame, Irreversible bone loss in osteomalacia. Comparison of radial photon absorptiometry with iliac bone histomorphometry during treatment. *J. Clin. Invest.* **76**, 2403–2412 (1985).
8. B. Dawson-Hughes, S. S. Harris, E. A. Krall, G. E. Dallal, Effect of calcium and vitamin D supplementation on bone density in men and women 65 years of age or older. *N. Engl. J. Med.* **337**, 670–676 (1997).
9. M. Priemel, C. von Domarus, T. O. Klatte, S. Kessler, J. Schlie, S. Meier, N. Proksch, F. Pastor, C. Netter, T. Streichert, K. Püschel, M. Amling, Bone mineralization defects and vitamin D deficiency: Histomorphometric analysis of iliac crest bone biopsies and circulating 25-hydroxyvitamin D in 675 patients. *J. Bone Miner. Res.* **25**, 305–312 (2010).
10. B. Demiaux, M. E. Arlot, M. C. Chapuy, P. J. Meunier, P. D. Delmas, Serum osteocalcin is increased in patients with osteomalacia: Correlations with biochemical and histomorphometric findings. *J. Clin. Endocrinol. Metab.* **74**, 1146–1151 (1992).
11. M. F. Holick, Resurrection of vitamin D deficiency and rickets. *J. Clin. Invest.* **116**, 2062–2072 (2006).
12. R. S. Weinstein, J. L. Underwood, M. S. Hutson, H. F. DeLuca, Bone histomorphometry in vitamin D–deficient rats infused with calcium and phosphorus. *Am. J. Physiol.* **246**, E499–E505 (1984).
13. A. Bhan, A. D. Rao, D. S. Rao, Osteomalacia as a result of vitamin D deficiency. *Endocrinol. Metab. Clin. North Am.* **39**, 321–331 (2010).
14. Y. Sato, J. Iwamoto, Y. Honda, Vitamin D deficiency-induced vertebral fractures may cause stooped posture in Parkinson disease. *Am. J. Phys. Med. Rehabil.* **90**, 281–286 (2011).
15. M. Bolland, A. Grey, A. Horne, M. Thomas, Osteomalacia in an HIV-infected man receiving rifabutin, a cytochrome P450 enzyme inducer: A case report. *Ann. Clin. Microbiol. Antimicrob.* **7**, 3 (2008).
16. E. A. Zimmermann, E. Schaible, H. Bale, H. D. Barth, S. Y. Tang, P. Reichert, B. Busse, T. Alliston, J. W. Ager III, R. O. Ritchie, Age-related changes in the plasticity and toughness of human cortical bone at multiple length scales. *Proc. Natl. Acad. Sci. U.S.A.* **108**, 14416–14421 (2011).
17. M. E. Launey, M. J. Buehler, R. O. Ritchie, On the mechanistic origins of toughness in bone. *Annu. Rev. Mater. Res.* **40**, 25–53 (2010).
18. K. J. Koester, J. W. Ager III, R. O. Ritchie, The true toughness of human cortical bone measured with realistically short cracks. *Nat. Mater.* **7**, 672–677 (2008).
19. H. D. Barth, E. A. Zimmermann, E. Schaible, S. Y. Tang, T. Alliston, R. O. Ritchie, Characterization of the effects of x-ray irradiation on the hierarchical structure and mechanical properties of human cortical bone. *Biomaterials* **32**, 8892–8904 (2011).
20. J. W. Ager, R. K. Nalla, K. L. Breeden, R. O. Ritchie, Deep-ultraviolet Raman spectroscopy study of the effect of aging on human cortical bone. *J. Biomed. Opt.* **10**, 034012 (2005).
21. P. Roschger, E. P. Paschalis, P. Fratzl, K. Klaushofer, Bone mineralization density distribution in health and disease. *Bone* **42**, 456–466 (2008).
22. M. F. Holick, T. C. Chen, Vitamin D deficiency: A worldwide problem with health consequences. *Am. J. Clin. Nutr.* **87**, 1080S–1086S (2008).
23. M. F. Holick, Too little vitamin D in premenopausal women: Why should we care? *Am. J. Clin. Nutr.* **76**, 3–4 (2002).
24. A. Boyde, E. Maconnachie, S. A. Reid, G. Delling, G. R. Mundy, Scanning electron microscopy in bone pathology: Review of methods, potential and applications. *Scan. Electron Microsc.* 1537–1554 (1986).
25. D. Schamall, M. Teschler-Nicola, F. Kainberger, St. Tangl, F. Brandstätter, B. Patzak, J. Muhsil, H. Plenk Jr., Changes in trabecular bone structure in rickets and osteomalacia: The potential of a medico-historical collection. *Int. J. Osteoarchaeol.* **13**, 283–288 (2003).
26. M. Brickley, S. Mays, R. Ives, An investigation of skeletal indicators of vitamin D deficiency in adults: Effective markers for interpreting past living conditions and pollution levels in 18th and 19th century Birmingham, England. *Am. J. Phys. Anthropol.* **132**, 67–79 (2007).
27. N. E. Lane, W. Yao, Glucocorticoid-induced bone fragility. *Ann. N. Y. Acad. Sci.* **1192**, 81–83 (2010).
28. D. W. Dempster, H. Y. Elder, W. A. Nicholson, D. A. Smith, V. A. Moss, Changes in bone mineral in experimentally induced rickets in the rat: Electron microprobe and chemical studies. *Calcif. Tissue Int.* **30**, 135–146 (1980).
29. M. Harris, D. J. F. Rowe, A. J. Darby, Anticonvulsant osteomalacia induced in the rat by diphenylhydantoin. *Calcif. Tissue Res.* **25**, 13–17 (1978).
30. B. E. C. Nordin, *Metabolic Bone and Stone Disease* (Churchill Livingstone, Edinburgh, 1973).
31. R. K. Nalla, J. J. Kruzic, J. H. Kinney, M. Balooch, J. W. Ager III, R. O. Ritchie, Role of microstructure in the aging-related deterioration of the toughness of human cortical bone. *Mater. Sci. Eng. C* **26**, 1251–1260 (2006).
32. For the enzymatic cross-links in collagen, this represents the ratio of the nonreducible mature (interfibrillar) divalent cross-links, pyridinoline (Pyd), to the reducible immature (intrafibrillar) divalent cross-links, dihydroxylysinonorleucine (deH-DHLNL).
33. M. E. Ruppel, D. B. Burr, L. M. Miller, Chemical makeup of microdamaged bone differs from undamaged bone. *Bone* **39**, 318–324 (2006).
34. A. L. Boskey, R. Coleman, Aging and bone. *J. Dent. Res.* **89**, 1333–1348 (2010).
35. D. Farlay, G. Panczer, C. Rey, P. D. Delmas, G. Boivin, Mineral maturity and crystallinity index are distinct characteristics of bone mineral. *J. Bone Miner. Metab.* **28**, 433–445 (2010).
36. A. Boskey, N. Pleshko Camacho, FT-IR imaging of native and tissue-engineered bone and cartilage. *Biomaterials* **28**, 2465–2478 (2007).
37. G. P. Parsamian, T. L. Norman, Diffuse damage accumulation in the fracture process zone of human cortical bone specimens and its influence on fracture toughness. *J. Mater. Sci. Mater. Med.* **12**, 779–783 (2001).
38. C. H. Turner, Biomechanics of bone: Determinants of skeletal fragility and bone quality. *Osteoporos. Int.* **13**, 97–104 (2002).
39. B. Busse, D. Djonic, P. Milovanovic, M. Hahn, K. Püschel, R. O. Ritchie, M. Djuric, M. Amling, Decrease in the osteocyte lacunar density accompanied by hypermineralized lacunar occlusion reveals failure and delay of remodeling in aged human bone. *Aging Cell* **9**, 1065–1075 (2010).
40. S. L. Teitelbaum, Renal osteodystrophy. *Hum. Pathol.* **15**, 306–323 (1984).
41. R. Brommage, S. C. Miller, C. B. Langman, R. Bouillon, R. Smith, J. E. Bourdeau, The effects of chronic vitamin D deficiency on the skeleton in the adult rabbit. *Bone* **9**, 131–139 (1988).
42. B. Busse, M. Hahn, M. Soltau, J. Zustin, K. Püschel, G. N. Duda, M. Amling, Increased calcium content and inhomogeneity of mineralization render bone toughness in osteoporosis: Mineralization, morphology and biomechanics of human single trabeculae. *Bone* **45**, 1034–1043 (2009).
43. M. Cochran, B. E. C. Nordin, Role of acidosis in renal osteomalacia. *Br. Med. J.* **2**, 276–279 (1969).
44. K. Sato, P. D. Byers, Quantitative study of tunneling and hook resorption in metabolic bone disease. *Calcif. Tissue Int.* **33**, 459–466 (1981).
45. H. M. Frost, The dynamics of human osteoid tissue, in *L'Ostéomalacie: Symposium Organisé par le Centre du Métabolisme Phospho-Calcique (Centre André-Lichtwitz), Tours*, D. J. Hioco, Ed. (Masson, Paris, 1967), pp. 3–18.
46. E. P. Paschalis, K. Verdelis, S. B. Doty, A. L. Boskey, R. Mendelsohn, M. Yamauchi, Spectroscopic characterization of collagen cross-links in bone. *J. Bone Miner. Res.* **16**, 1821–1828 (2001).
47. C. von Domarus, J. Brown, F. Barvencik, M. Amling, P. Pogoda, How much vitamin D do we need for skeletal health? *Clin. Orthop. Relat. Res.* **469**, 3127–3133 (2011).
48. P. Bordier, H. Matrajt, L. Miravet, D. Hioco, Histological measure of the volume and resorption of bone joints. *Pathol. Biol.* **12**, 1238–1243 (1964).
49. A. M. Parfitt, M. K. Drezner, F. H. Glorieux, J. A. Kanis, H. Malluche, P. J. Meunier, S. M. Ott, R. R. Recker, Bone histomorphometry: Standardization of nomenclature, symbols, and units. Report of the ASBMR Histomorphometry Nomenclature Committee. *J. Bone Miner. Res.* **2**, 595–610 (1987).
50. N. Fratzl-Zelman, P. Roschger, B. M. Misof, S. Pfeffer, F. H. Glorieux, K. Klaushofer, F. Rauch, Normative data on mineralization density distribution in iliac bone biopsies of children, adolescents and young adults. *Bone* **44**, 1043–1048 (2009).
51. L. M. Miller, V. Vairavamurthy, M. R. Chance, R. Mendelsohn, E. P. Paschalis, F. Betts, A. L. Boskey, In situ analysis of mineral content and crystallinity in bone using infrared micro-spectroscopy of the ν_4 PO_4^{3-} vibration. *Biochim. Biophys. Acta* **1527**, 11–19 (2001).
52. ASTM E1820-08, *Annual Book of ASTM Standards: Metals—Mechanical Testing; Elevated and Low-Temperature Tests; Metallography* (ASTM International, West Conshohocken, PA, 2008).
53. B. Cotterell, J. R. Rice, Slightly curved or kinked cracks. *Int. J. Fract.* **16**, 155–169 (1980).

Acknowledgments: We thank T. Tomsia for his support. **Funding:** In Berkeley, this work was supported by the Laboratory Directed Research and Development Program of Lawrence Berkeley National Laboratory (LBNL), funded by the U.S. Department of Energy under grant no. DE-AC02-05CH11231. We acknowledge the use of the x-ray synchrotron beamline 8.3.2 (microtomography) and the FTIR beamline 1.4.3 at the ALS at LBNL, which is supported by

the Office of Science of the U.S. Department of Energy under contract. In Hamburg, this work was funded by the Federal Ministry of Education and Research through the consortium "Osteopath" (01 EC 1006F). B.B. is a fellow of the Deutsche Forschungsgemeinschaft (BU 2562/2-1). **Author contributions:** B.B., M.A., and R.O.R. designed the study. B.B., H.A.B., E.A.Z., B.P., A.C., and J.W.A. performed the experiments. B.B., H.A.B., E.A.Z., J.W.A., M.A., and R.O.R. analyzed the data. E.A.Z., H.A.B., H.D.B., and J.W.A. contributed reagents or analytic tools. K.P. performed autopsies. E.V., J.Z., and M.H. gave technical support and conceptual advice. B.B., E.A.Z., and R.O.R. wrote the manuscript. **Competing interests:** The authors declare that they have no competing interests.

Submitted 3 April 2013
Accepted 18 June 2013
Published 10 July 2013
10.1126/scitranslmed.3006286

Citation: B. Busse, H. A. Bale, E. A. Zimmermann, B. Panganiban, H. D. Barth, A. Carriero, E. Vettorazzi, J. Zustin, M. Hahn, J. W. Ager III, K. Püschel, M. Amling, R. O. Ritchie, Vitamin D deficiency induces early signs of aging in human bone, increasing the risk of fracture. *Sci. Transl. Med.* **5**, 193ra88 (2013).